NANO LETTERS

Letter

pubs.acs.org/NanoLett

Atomic and Electronic Structure of the $BaTiO_3$/Fe Interface in Multiferroic Tunnel Junctions

Laura Bocher,[†] Alexandre Gloter,*[,†] Arnaud Crassous,[‡] Vincent Garcia,[‡] Katia March,[†] Alberto Zobelli,[†] Sergio Valencia,[§] Shaïma Enouz-Vedrenne,[∥] Xavier Moya,[⊥] Neil D. Marthur,[⊥] Cyrile Deranlot,[‡] Stéphane Fusil,[‡] Karim Bouzehouane,[‡] Manuel Bibes,[‡] Agnès Barthélémy,[‡] Christian Colliex,[†] and Odile Stéphan[†]

[†]Laboratoire de Physique des Solides, Bâtiment 510, CNRS UMR 8502, Université Paris Sud XI, 91405 Orsay, France

[‡]Unité Mixte de Physique CNRS, Thales associée à l'Université Paris Sud XI, Campus de l'Ecole Polytechnique, 1 Avenue A. Fresnel, 91767 Palaiseau, France

[§]Helmholtz-Zentrum-Berlin für Materialien und Energie, Albert-Einstein-Strasse 15, 12489 Berlin, Germany

[∥]Thales Research and Technology, Campus de l'Ecole Polytechnique, 1 Avenue A. Fresnel, 91767 Palaiseau, France

[⊥]Department of Materials Science, University of Cambridge, Cambridge CB23QZ, United Kingdom

Supporting Information

ABSTRACT: Artificial multiferroic tunnel junctions combining a ferroelectric tunnel barrier of $BaTiO_3$ with magnetic electrodes display a tunnel magnetoresistance whose intensity can be controlled by the ferroelectric polarization of the barrier. This effect, called tunnel electromagnetoresistance (TEMR), and the corollary magnetoelectric coupling mechanisms at the $BaTiO_3$/Fe interface were recently reported through macroscopic techniques. Here, we use advanced spectromicroscopy techniques by means of aberration-corrected scanning transmission electron microscopy (STEM) and electron energy-loss spectroscopy (EELS) to probe locally the nanoscale structural and electronic modifications at the ferroelectric/ferromagnetic interface. Atomically resolved real-space spectroscopic techniques reveal the presence of a single FeO layer between $BaTiO_3$ and Fe. Based on this accurate description of the studied interface, we propose an atomistic model of the ferroelectric/ferromagnetic interface further validated by comparing experimental and simulated STEM images with atomic resolution. Density functional theory calculations allow us to interpret the electronic and magnetic properties of these interfaces and to understand better their key role in the physics of multiferroics nanostructures.

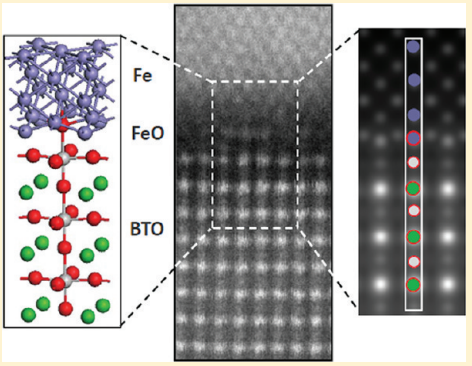

KEYWORDS: *Atomically resolved EELS, aberration-corrected STEM, multiferroic nanojunctions, ab initio calculations*

The design of room-temperature multiferroic materials and nanoscale architectures currently generates strong theoretical and experimental efforts in condensed matter physics as well as in the development of upcoming spintronic devices.[1,2] Examples of such nanoelectronic devices include artificial multiferroic tunnel junctions (MFTJs)[3] in which magnetic and spin-dependent transport properties can be electrically controlled in a nonvolatile way, enabling low-power information write operations in magnetic random access memories. These heterostructures combine ferromagnetic (FM) electrodes and a ferroelectric (FE) insulator as the tunnel barrier. As such, their tunnel resistance is expected to depend on the magnetic and ferroelectric orders, i.e., they display tunnel magnetoresistance (TMR) and tunnel electroresistance (TER) effects, respectively, giving rise to four resistance states.

In addition, novel magnetoelectric phenomena at FE/FM interfaces have recently emerged as the pivotal point in such nanojunctions, with potentially emerging interfacial phases revealing unusual electronic properties.[3] These interfacial magnetoelectric effects may show up as a modulation of the spin polarization by ferroelectricity at FE/FM interfaces and the corollary induction of a finite magnetic moment in the FE. Interface mechanisms at the origin of such magnetoelectric coupling were first theoretically predicted by Duan et al. for the $BaTiO_3$/Fe system.[4] Recently, Garcia et al. demonstrated the nonvolatile electrical control of the TMR in artificial $La_{2/3}Sr_{1/3}MnO_3/BaTiO_3$/Fe (LSMO/BTO/Fe) MFTJs after switching the electrical polarization of the tunnel barrier, reflecting the modulation of the carriers spin polarization by the direction of FE polarization.[5] In addition, experimental evidence of remanent induced magnetic moments on Ti and O atoms coupled with those of Fe was more recently observed

Received: October 17, 2011
Revised: December 16, 2011

 © XXXX American Chemical Society dx.doi.org/10.1021/nl203657c | *Nano Lett.* XXXX, XXX, XXX–XXX

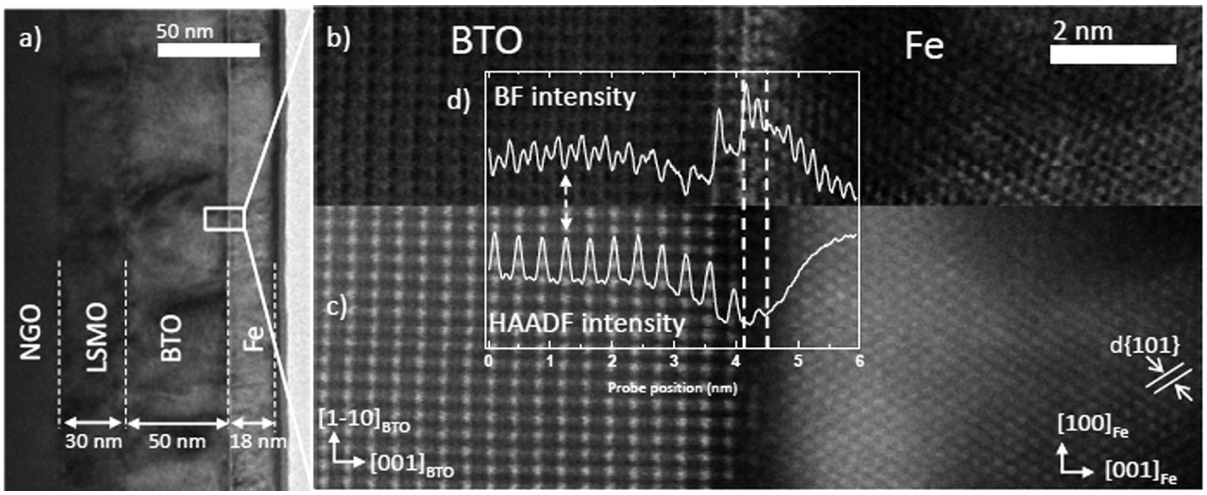

Figure 1. (a) Low-magnification TEM image of the NGO(001)//LSMO(30 nm)/BTO(50 nm)/Fe(18 nm) nanojunction; (b) and (c) simultaneously acquired atomically resolved BF and HAADF STEM images of the BTO/Fe interface, respectively; and (d) overlayered BF and HAADF averaged intensity profiles. $BaTiO_3$ is projected onto the $[110]_{BTO}$ zone axis, while the Fe layer is oriented along the $[010]_{Fe}$ zone axis.

in analogous LSMO/BTO/Fe MFTJs by means of X-ray resonant magnetic scattering (XRMS) measurements.[6] However, these averaging real-space techniques are not sensitive enough to probe pure atomic and electronic interfacial properties in those artificial MFTJs. Moreover, in view of the extreme sensitivity of both tunneling and induced magnetic moments to the interface details, a precise knowledge of the atomic scale structure is a key prerequisite to understand the physics of multiferroic junctions.

Recently, precise atomically resolved investigations of low-dimensional systems, such as artificial nanojunctions, have risen up thanks to fundamental technological breakthroughs in electron microscopy with the correction of electron-optical aberrations paving the way toward sub-Angström spatial resolution.[7] Beyond looking at atom positions, 2D elemental mapping of ,e.g., full-perovskite-type oxide heterostructures, has been achieved when coupled with spectroscopic capabilities.[8,9] Moreover, core-level electron energy-loss spectroscopy (EELS) provides local electronic information at the same spatial resolution. For instance, fine structure EELS investigations of nanoscale systems involving transition-metal 2p → 3d excitations can yield valence state quantification, information on charge transfer, or crystal field modification at the atomic scale.[10,11]

In this Letter, using new-generation aberration-corrected scanning transmission electron microscopy (STEM),[7] we demonstrate that subtle local structural and electronic modifications at FE/FM interfaces have a fundamental impact on the spin polarization modulation based on interfacial properties. More precisely, we report on a comprehensive experimental and theoretical atomic investigation at the oxide/metal interface in these specific LSMO/BTO/Fe MFTJs. We first present an in-depth and precise structural, chemical, and electronic study of the BTO/Fe interface. Through atomically resolved STEM investigations combined with high-energy resolution EELS, we resolve the interfacial stacking sequence. Energy-loss near-edge structures (ELNES) of the Fe-$L_{2,3}$ edges emphasize different spectroscopic signatures on single atomic column when probing, with the highest resolution and sensitivity, the interface and the metallic electrode. Based on these experimental findings, and confirmed by image simulations, we further propose an accurate description of the interface structure different from that previously theoretically suggested,[4,12] i.e., where an additional FeO monolayer is intercalated between $BaTiO_3$ and Fe. First principle calculations of atomic and spin-dependent electronic structures enable us to demonstrate that the FE control of magnetism can also occur in a FeO-terminated BTO/Fe interface. Comparison of the predicted FE polarization-dependent spin-resolved density of states (DOS) with the measured FE polarization-dependent TMR sheds more light on the precise microscopic mechanism responsible for the TEMR effect.

The investigated nanojunctions are based on $La_{2/3}Sr_{1/3}MnO_3/BaTiO_3$ bilayers grown by pulsed laser deposition on (001)-oriented $NdGaO_3$ substrates, the counterpart electrode of Fe was grown ex situ by radio frequency (RF) sputtering.[5,13] Microscopy studies were performed on cross-sectional views of NGO(001)//LSMO/BTO/Fe heterostructures using a Cs aberration-corrected STEM, the NION UltraSTEM100 equipped with a cold-field emission electron source operated at 100 kV and coupled with a high-resolution EEL spectrometer enabling an energy resolution of 350 meV in the core-loss region. First principle calculations were performed within the density functional theory (DFT) using the ABINIT code. DFT calculations were carried out using a plane-wave basis set limited by a cutoff energy of 50 hartree using a pseudopotential approach with nonlinear core correction and a local spin density approximation. Image simulations were carried out based on the multislice method[14] using the QSTEM package. The tunnel junctions were defined by nanoindentation lithography.[15]

In these artificial LSMO/BTO/Fe nanojunctions, we first precisely investigate the atomic structure of the FE/FM interface which is believed to be at the origin of the magnetoelectric coupling. The low-magnification TEM image in Figure 1a shows an overview of a NGO(001)//LSMO(30 nm)/BTO(50 nm)/Fe(18 nm) heterostructure with all the layers resulting from a homogeneous and controlled growth process.[13] No structural defects are observed at this spatial resolution. Atomically resolved bright-field (BF) and high-angle annular dark-field (HAADF) STEM images of the BTO/Fe interface are presented in Figure 1b,c. The BTO layer is characterized by a well-defined epitaxial growth.[5,13] The TiO_6 octahedra can be identified in the BF image, while the Ba atoms

dx.doi.org/10.1021/nl203657c | Nano Lett. XXXX, XXX, XXX–XXX

are clearly pinpointed as the brighter spots in the HAADF image. More quantitatively, the BF intensity profile of the BTO lattice emphasizes broad double peaks corresponding to the TiO_6 octahedra, while the HAADF profile depicts narrow maxima indicating the BaO column positions. The FM layer is characterized by {101} bcc Fe lattice fringes. The topotactic relationship of the studied interface corresponds to $[1-10]_{BTO} \leftrightarrow [100]_{Fe}$ and $[001]_{BTO} \leftrightarrow [001]_{Fe}$. The HAADF image reveals a darker contrast between the oxide and the metallic layers extending over less than one nanometer. This is confirmed in the HAADF profile by a general decrease of the background and the signal toward the interface. In the corresponding BF intensity profile, a last double peak, indicating the presence of a BO_6 octahedra, is distinguished in this region. This suggests that the interfacial region between the BTO and the Fe layers consists of a perovskite-type unit cell, however, slightly chemically different from the BTO structure.

Atomically resolved EELS-based elemental profiles of the Ba-$M_{4,5}$, Ti-$L_{2,3}$, Fe-$L_{2,3}$, and O-K edges acquired across the BTO/Fe interface are shown in Figure 2a. The perovskite lattice is

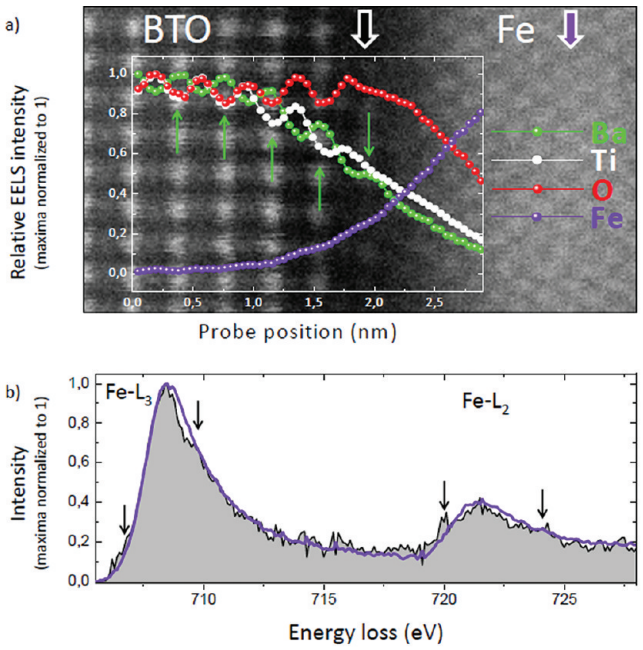

Figure 2. (a) Ba, Ti, O, and Fe profiles (green, white, red, and violet dotted lines, respectively) obtained from EELS spectra acquired across the interface; (b) ELNES spectra acquired at the Fe layer (violet line) and at the interface (black line), as approximately indicated by the colored arrows in (a). The background HAADF image is intended to guide the eye. The elemental profiles were extracted after applying (i) a principal component analysis (PCA) on EEL spectra to reduce the contribution of random noise and (ii) a power-law background subtraction. In (b) black arrows indicate multiplet features characteristics of Fe^{2+} and Fe^{3+} contributions.[14]

characterized by a clear anticorrelation between the extracted profiles of the BaO and TiO_2 columns. In the interfacial region, both Ba and Ti signals strongly diminish toward the FM layer while the presence of oxygen remains, and the Fe profile starts to rise before probing the Fe lattice. The simultaneous presence of Fe and Ba is clearly confirmed in this area (Figure S1a–c, Supporting Information). These findings corroborate the presence of an interfacial phase between the FE/FM layers.

The Fe electronic structure was probed at the interface and in the Fe layer by means of high-energy resolved ELNES at the Fe-$L_{2,3}$ edges (Figure 2b). The ELNES spectrum acquired in the Fe bulk region displays broad and asymmetric Fe-$L_{2,3}$ edges characteristic of metallic Fe.[16] On the contrary, the spectrum extracted from the interface presents multiplet features typical of Fe^{2+} (pre-edge at around 707 eV) and Fe^{3+} contributions (marked feature at around 710 eV). This finding indicates the presence of oxidized iron at the interface, most probably, over solely one atomic column. As confirmed by linear combinations of $Fe/Fe^{2+}/Fe^{3+}$ reference spectra,[16] Fe^{2+} turns out to be the major ionic contribution (Figure S1d, Supporting Information). Previous X-ray absorption spectroscopy (XAS) and X-ray magnetic circular dichroism (XMCD) measurements acquired on similar nanojunctions could not detect the presence of less than two oxidized iron monolayers.[5,17] ELNES at the Ti-$L_{2,3}$ edges (Figure S1f, Supporting Information) are typical of Ti^{4+} cations in the BTO layer as well as at the interface, in agreement with XAS results obtained in these heterostructures.[5] Complementary investigations on NGO//LSMO/BTO/Fe nanojunctions with a 3.5 nm BTO layer yield similar structural, chemical, and electronic features at the oxide/metal interface (Figure S2, Supporting Information). Based on these experimental results acquired at the atomic scale, roughness effects at the oxide/metal interface do not appear responsible for the dark contrast observed in the HAADF image in the specific case of these studied interfaces.

These results reveal a more complex atomic and electronic structure of the studied interface than the ideal model considered in earlier theoretical studies.[4,12] The archetypal interface (model I) considered in these previous works consists of a TiO_2-terminated surface with interfacial apical O atoms aligned along the Fe sites. In line with our experimental results, we propose three alternative structural models of the FE/FM interface, i.e., models II, III, and IV (Figure 3c–f and Figure S3, Supporting Information for detailed schematic representations). The proposed models can be regarded as oxidized-type interfaces involving an additional monolayer where interfacial Fe atoms are hybridized with O atoms also in the interfacial plane. The interface models II and III present TiO_2-termination planes (layer L_{+1}) neighbored by a FeO monolayer where Fe atoms are either located atop sites along the BaO columns (model II) or along the apical O atoms (model III). The interface model IV is BaO/FeO_2-terminated where interfacial apical O atoms are aligned with the Fe sites. Based on the above-reported spectroscopic evidence, interface models II and III are more likely to explain the present results as they involve a Fe^{2+}-terminated surface. These models were structurally relaxed by energy minimization through first principle calculations, and image simulations were performed based on relaxed atomic positions enabling us a comparison with the experimental atomically resolved HAADF image (Figure 3). Experimental and simulated images present a good agreement concerning the BTO and the Fe lattices, while different image contrasts are visible in the interfacial region depending on the proposed model (Figure 3g–j). Intensity profiles extracted along the BaO-TiO_2 column allow us to determine precisely the correct structural model (Figure 3k–n). The interfacial region consists of two defined atomic planes of ca. 4 and 2 Å (Figure 3b), the larger one roughly corresponding to the perovskite unit cell. Intensity profiles obtained from the simulated images of the interface models III and IV as well as that one corresponding to the ideal interface do not fit with the

dx.doi.org/10.1021/nl203657c | Nano Lett. XXXX, XXX, XXX–XXX

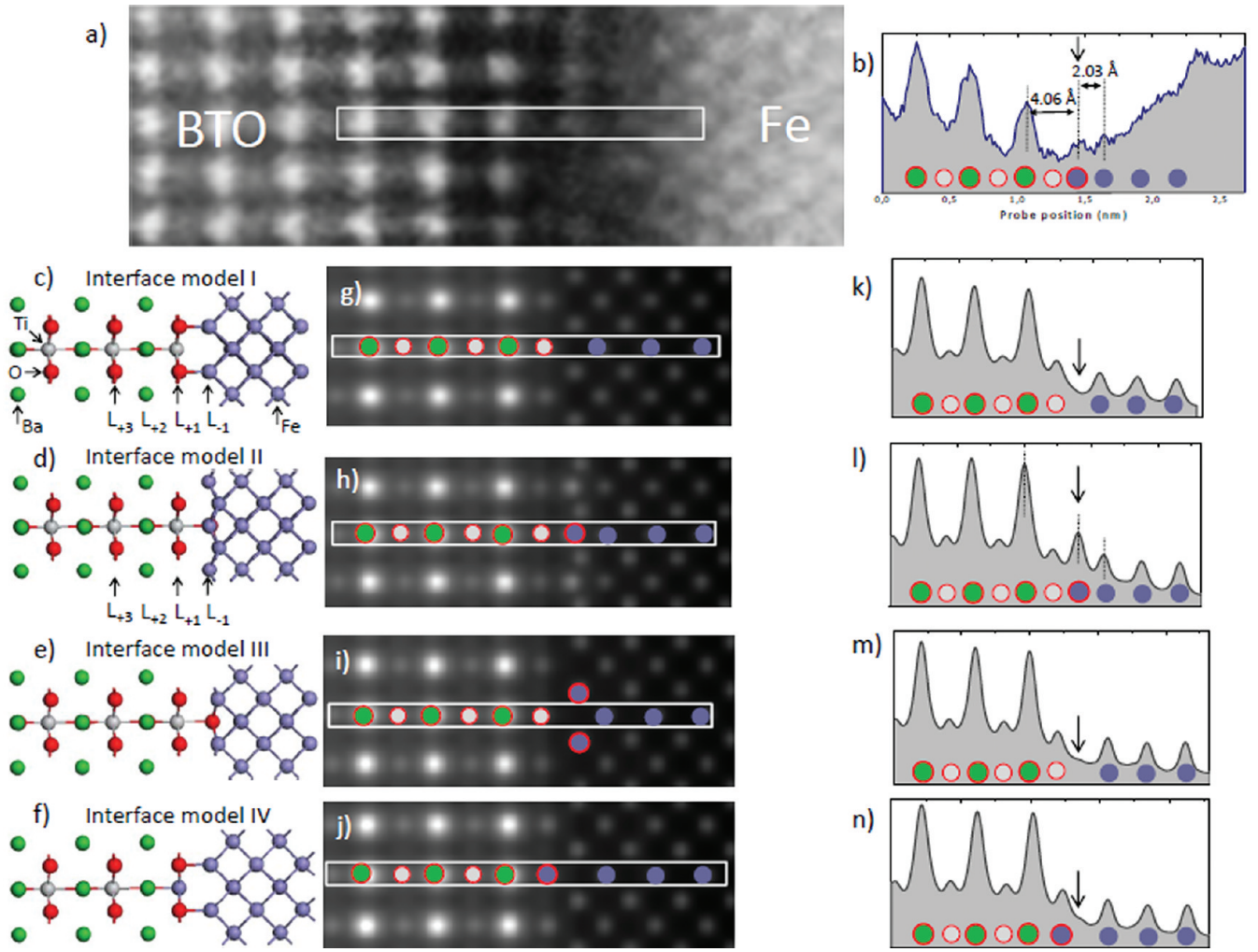

Figure 3. (a) Experimental image of the interface and (b) the corresponding profile extracted along a BaO-TiO_2 column from the white rectangle in (a). (c–f) Interface models projected onto the $[110]_{BTO}$ zone axis. (g–j) Simulated images and (k–n) corresponding profiles picked up over the white rectangle area. The positions of the BaO (green/red circles), TiO_2 (gray/red circles), FeO (or FeO_2) (violet/red circles), and Fe (violet circles) atomic columns are indicated in the simulated images and along the profiles. Arrows in (k–n) indicate the position of an atomic column experimentally observed in Figure b.

experimental data. They do not reproduce the increase of intensity clearly observed for the probe position at approximately 1.5 nm, as indicated by arrows in Figure 3k–n. The model matching better with the experimental profile is the interface model II, since here interfacial Fe atoms located atop on the O apical atoms are aligned along the BaO-TiO_2 columns yielding atomic planes separated by approximately 2 Å (Figure 3h).

In the frame of our experimental and simulation results, we consider the oxidized interface (model II) as the most likely to describe our nanofabricated MFTJs. This highlights the questions of whether the ferroelectric control of interfacial magnetism[5,6] can be efficiently preserved in such configuration and how a FeO monolayer can influence the electronic and magnetic properties at the interface. DFT calculations on the interface models I and II were performed to understand better the origin of the transport and magnetic properties at the FE/FM interface and to highlight the differences between the ideal and oxidized interfaces. We first investigate the cationic/anionic displacements in the BTO lattice obtained after structural relaxations (Table 1). Both models yield polar atomic displacements up to the interface. In the oxidized model, the

Table 1. Ab initio Calculated Cationic/Anionic Displacements, i.e., $\delta = z_{cation} - z_O$ (in Å), in BTO for Both Polarization Configurations[a]

	type I interface		type II interface	
	P_{up}	P_{down}	P_{up}	P_{down}
Ti (L_{+1})	0.078	−0.101	0.052	−0.185
Ba (L_{+2})	0.090	−0.110	0.049	−0.126
Ti (L_{+3})	0.093	−0.133	0.069	−0.147

[a]The bulk BTO structure yields $\delta_{Ti/O} = 0.148$ Å and $\delta_{Ba/O} = 0.101$ Å in the FE state.

FE character is still preserved corroborating previous experimental findings in analogous heterostructures.[5,13] Fechner et al. theoretically predicted for the ideal interface a depolarizing effect toward the interface resulting in an asymmetric trend depending on the FE polarization direction, i.e., the FE polarization pointing toward the interface (P_{up}) induces larger atomic displacements.[12] This asymmetric evolution is more pronounced in the oxidized interface. Table 2 compares calculated magnetic moments of interfacial Fe, Ti, and O atoms for both models, results obtained for the interface

dx.doi.org/10.1021/nl203657c | Nano Lett. XXXX, XXX, XXX–XXX

Table 2. Ab initio Calculated Magnetic Moments (in μ_B) of Interfacial Fe, Ti, and O Atoms for Both Polarization Configurations[a]

	interface model I					interface model II				
	Fe [P_{up}]	2.07					Fe [P_{up}]	2.09			
Fe (L_{-3})	Fe [P_{down}]	2.06				Fe (L_{-3})	Fe [P_{down}]	2.05			
	Δ μFe	>0.01					Δ μFe	0.04			
	Fe [P_{up}]	2.04					Fe [P_{up}]	2.35			
Fe (L_{-2})	Fe [P_{down}]	2.08				Fe (L_{-2})	Fe [P_{down}]	2.34			
	D μFe	−0.04					Δ μFe	0.01			
	Fe [P_{up}]	2.12					Fe [P_{up}]	2.85		O [P_{up}]	0.18
Fe (L_{-1})	Fe [P_{down}]	2.31				Fe (L_{-1})	Fe [P_{down}]	2.76	O (L_{-1})	O [P_{down}]	0.15
	Δ μFe	−0.19					Δ μFe	0.09		Δ μO	0.03
	Ti [P_{up}]	−0.19		O [P_{up}]	0.037		Ti [P_{up}]	−0.06		O [P_{up}]	0.040
Ti (L_{+1})	Ti [P_{down}]	−0.09	O (L_{+1})	O [P_{down}]	0.046	Ti (L_{+1})	Ti [P_{down}]	−0.09	O (L_{+1})	O [P_{down}]	0.066
	Δ μTi	−0.10		Δ μO	−0.009		Δ μTi	0.03		Δ μO	−0.026

[a] Δμ is the difference between the magnetic moments when the polarization is pointing toward and away from Fe.

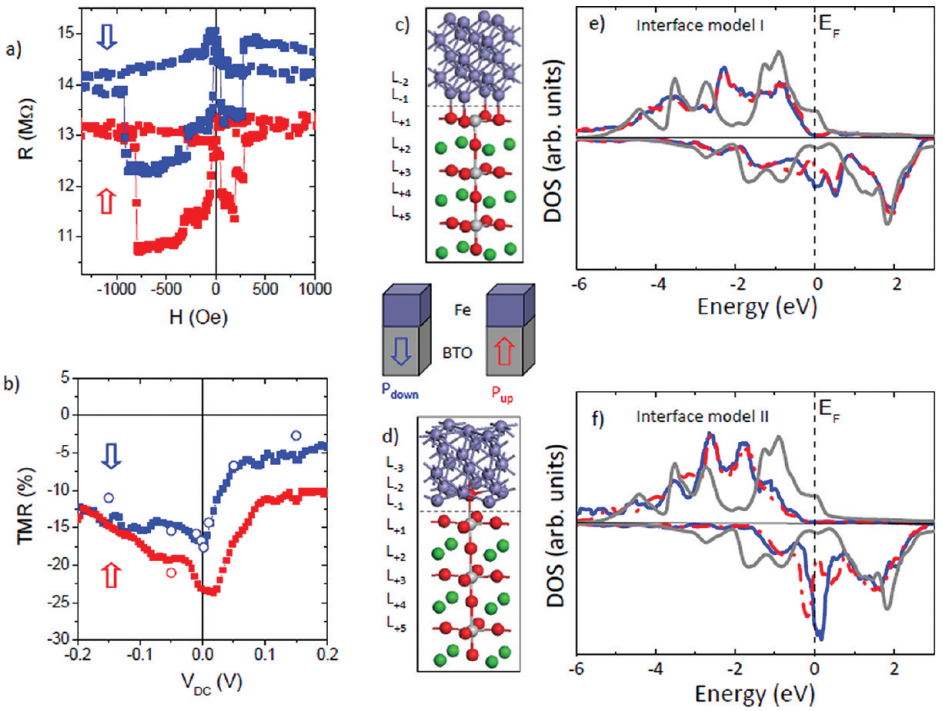

Figure 4. (a) R(H) for the LSMO/BTO(1 nm)/Fe junction at V_{DC} = −50 mV and (b) TMR as function of the applied voltage from V_{DC} from $I(V_{DC})$ (full dots) and R(H) (open dots) for the LSMO/BTO(1 nm)/Fe junction for both polarization orientations P_{up}/P_{down} (red/blue lines). (c−f) Structural models and spin-resolved DOS of the interfacial Fe(L_{-1}) 3d atoms with the P_{up}/P_{down} (dashed red/solid blue lines) for the interface models I and II, respectively. The gray line corresponds to the DOS of Fe bulk.

I being in good agreement with previous reported calculations.[4,12] For both models, Fe magnetic moments increase toward the interface. The first interfacial Fe(L_{-1}) atoms carry larger moments at the interface model II than in the ideal case due to its partial oxidation (2.80 μB in average for interface-type II and 2.20 μB for interface-type I);[6] those values being still lower than for Fe(100) surface (2.98 μB). Besides, in both cases, a significant asymmetry of the magnetism behavior is observed in this Fe(L_{-1}) layer depending on the polarization orientation, since the interface-induced ferroelectricity implies a strong structural sensitivity.[4] Likewise the Fe(L_{-2}) atoms carry enhanced moments in the interface model II compared to the bulk, and their DOS (not shown here) resemble that one of Fe(L_{-1}) atoms in the interface model I. The Fe(L_{-3}) atoms are obviously less influenced by the FE polarization. More importantly, interfacial Ti and O atoms present, in each case, sizable induced moments coupled to Fe (consistent with the results obtained by XRMS measurements by Valencia et al.),[6] antiferromagnetically and ferromagnetically oriented with respect to Fe, respectively. These magnetic moments induced on interfacial Ti and O atoms result from the hybridization of the Fe 3d band with the Ti 3d and O 2p bands, as depicted in the spin-resolved DOS (Figure S4, Supporting Information). In the interface-type I characterized by a TiO_2-terminated surface, the strong Ti 3d band which overlaps with the minority-spin Fe 3d band near the Fermi level (E_F) is at the origin of the development of induced magnetic moments on Ti(L_{+1}) atoms. In contrast a large overlap between the O 2p and the majority-spin Fe 3d states is observed for the interface model II due to the direct hybridization in the plane direction

dx.doi.org/10.1021/nl203657c | Nano Lett. XXXX, XXX, XXX−XXX

between O(L_{-1}) and Fe(L_{-1}) atoms, implying larger moments on oxygen atoms. Ti(L_{+1}) atoms of the oxidized interface are in an octahedral environment promoting a complete charge transfer between the Ti 3d and O 2p orbitals. This would also explain the observation of solely Ti^{4+} cations at the interface by ELNES (Figure S1f, Supporting Information) and provides theoretical and experimental evidence that induced magnetism on interfacial Ti atoms originates from Ti^{4+} cations.[6]

The spin-polarization of the Fe(L_{-1}) atoms develops also noticeable differences in both models. The interface model I presents a negative spin-polarized Fe DOS (Figure 4e), as previously reported.[4,12] The P_{down} polarization induces a larger DOS in the minority spin at the vicinity of E_F (up to ±300 meV from E_F). More generally, our results reproduce well all the trends in the spin-polarized DOS found by Duan et al. and Fechner et al. In the case of Ti-based perovskite/metal interfaces, the spin-polarization of the tunneling current is expected to be proportional to the interfacial spin-dependent DOS in first approximation.[18−20] The minority-spin DOS intensity near E_F is therefore expected to control the conductance of the studied LSMO/BTO/Fe MFTJs. Hence in the interface model I, larger negative TMR should occur in the P_{down} configuration in contrast with the experimental results that display a larger negative TMR for the P_{up} orientation (Figure 4a,b).

The oxidized model displays also a marked negatively spin-polarized interface (Figure 4f) characterized by a narrower energy bandwidth than in the ideal interface which can be expected for partially oxidized Fe environment since stronger correlations should occur. Notably, this narrow DOS distribution in the minority spin is located at a different energy for both polarization configurations, i.e., the Fe 3d distribution being lower in energy in the P_{up} orientation. The calculated E_F position does not quantitatively predict which polarization direction should yield the largest spin polarization since E_F is located at a crossing point of the DOS for both orientations. Indeed, the computed E_F position on such a system strongly depends on the Fe band exchange splitting, that can vary of ca. 100 meV, due to, e.g., slight strain changes (even of few percent),[21] or by considering a different functional.[22] However, for the interface model II, the spin polarization is predicted to be larger in the P_{up} configuration over 200−300 meV below E_F. In contrast with the interface model I, this situation is more consistent with the observation of a larger TMR up to about 200 mV for this polarization direction (Figure 4b, positive bias). This qualitative agreement between the DOS fine structures and the magnetotransport trends for the oxidized interface emphasizes the key role of the FeO monolayer and the importance of detailed investigations of the interfacial atomic structure to capture the complex physics of multiferroic and magnetoelectric architectures.

In summary, we have performed atomically resolved STEM and EELS investigations to determine a realistic interface model for the BTO/Fe interface and used it as an input in first principle calculations to understand in detail the magnetic and electronic properties of the interface. Our analysis evidences the subtle but fundamental role of an intermediate FeO monolayer between BTO and Fe. Spin-resolved DOS and atomically resolved magnetic moment calculations show a fair agreement with experimental results, thereby demonstrating how advanced real-space spectromicroscopy is a powerful technique, sensitive enough to probe precise and crucial atomic and electronic information at interfaces. Further combined with theoretical investigations, our experimental results enable us to interpret better the physics of nanoscale multiferroic systems and will hopefully stimulate in the future new theoretical considerations on the role of FE/FM interfaces at the atomic scale.

■ ASSOCIATED CONTENT

Supporting Information

The EELS fine structures analysis and the quantitative fitting of Fe-2p edges are reported. Structural models of oxidized interfaces are detailed. Densities of states for Fe-d, Ti-d and O-p of interfacial atoms are also reported. This material is available free of charge via the Internet at http://pubs.acs.org.

■ AUTHOR INFORMATION

Corresponding Author

*E-mail: alexandre.gloter@u-psud.fr.

■ ACKNOWLEDGMENTS

The authors acknowledge financial support from the European Union under the Framework 6 program under a contract for an Intergrated Infrastructure Initiative (reference 026019 ESTEEM) and the French METSA microscopy program, the France-UK PMC Alliance program, French RTRA Triangle de la Physique, UK EPSRC EP/E026206/I, French C-Nano Île de France, French ANR Oxitronics and the European Research Council Advanced grant project FEMMES (no. 267579). X.M. acknowledges support from Herchel Smith Postdoctoral Fellowship Fund.

■ REFERENCES

(1) Tsymbal, E. Y.; Kohlstedt, H. *Science* **2006**, *313*, 181−183.
(2) Bibes, M.; Barthélémy, A. *Nat. Mat.* **2008**, *7*, 425−426.
(3) Bibes, M.; Villegas, J. E.; Barthélémy, A. *Adv. Phys.* **2011**, *60*, 5−84.
(4) Duan, C.-G.; Jaswal, S. S.; Tsymbal, E. Y. *Phys. Rev. Lett.* **2006**, *97*, No. 047201.
(5) Garcia, V.; Bibes, M.; Bocher, L.; Valencia, S.; Kronast, F.; Crassous, A.; Moya, X.; Enouz-Vedrenne, S.; Gloter, A.; Imhoff, D.; Deranlot, C.; Marthur, N. D.; Fusil, S.; Bouzehouane, K.; Barthélémy, A. *Science* **2010**, *327*, 1106−1110.
(6) Valencia, S.; Crassous, A.; Bocher, L.; Garcia, V.; Moya, X.; Cherifi, R. O.; Deranlot, C.; Bouzehouane, K.; Fusil, S.; Zobelli, A.; Gloter, A.; Mathur, N. D.; Gaupp, A.; Abrudan, R.; Radu, F.; Barthélémy, A.; Bibes, M. *Nat. Mat.* **2011**, *10*, 753−759.
(7) Krivanek, O. L.; Corbin, G. J.; Dellby, N.; Elston, B. F.; Keyse, R. J.; Murfitt, M. F.; Own, C. S.; Szilagyi, Z. S.; Woodruff, J. W. *Ultramiscroscopy* **2008**, *108*, 179−195.
(8) Fitting Kourkoutis, L.; Xin, H. L.; Higuchi, T.; Hotta, Y.; Lee, J. H.; Hikita, Y.; Schlom, D. G.; Hwang, H. Y.; Muller, D. A. *Philos. Mag.* **2010**, *90*, 4731−4749.
(9) Sefrioui, Z.; Visani, C.; Calderón, M. J.; March, K.; Carrétéro, C.; Walls, M.; Rivera-Calzada, A.; León, C.; Lopez Anton, R.; Charlton, T. R.; Cuellar, F. A.; Iborra, E.; Ott, F.; Imhoff, D.; Brey, L.; Bibes, M.; Santamaria, J.; Barthélémy, A. *Adv. Mater.* **2010**, *22*, 5029−5034.
(10) Shah, A. B.; Ramasse, Q. M.; Zhai, X.; Wen, J. G.; May, S. J.; Petrov, I.; Bhattacharya, A.; Abbamonte, P.; Eckstein, J. N.; Zuo, J.-M. *Adv. Mater.* **2010**, *22*, 1156−1160.
(11) Shao, Y.; Maunders, C.; Rossouw, D.; Kolodiazhnyi, T.; Botton, G. A. *Ultramicroscopy* **2010**, *110*, 1014−1019.
(12) Fechner, M.; Maznichenko, I. V.; Ostanin, S.; Ernst, A.; Henk, J.; Bruno, P.; Mertig, I. *Phys. Rev. B* **2008**, *78*, No. 212406.
(13) Garcia, V.; Fusil, S.; Bouzehouane, K.; Enouz-Vedrenne, S.; Marthur, N. D.; Barthélémy, A.; Bibes, M. *Nature* **2009**, *460*, 81−84.
(14) Koch, C., Ph.D. dissertation; Arizona State University: Tempe, AZ, 2002.

(15) Bouzehouane, K.; Fusil, S.; Bibes, M.; Carrey, J.; Blon, T.; Le Dû, M.; Seneor, P.; Cros, V.; Vila, L. *Nano Lett.* **2003**, *3*, 1599−1602.
(16) Gloter, A.; Zbinden, M.; Guyot, F.; Gaill, F.; Colliex, C. *Earth Planet. Sci. Lett.* **2004**, *222*, 947−957.
(17) Abrudan, R.; Miguel, J.; Bernien, M.; Tieg, C.; Piantek, M.; Kirschner, J.; Kuch, W. *Phys. Rev. B* **2008**, *77*, No. 014411.
(18) Jullière, M. *Phys. Lett. A.* **1975**, *54*, 225−226.
(19) De Teresa, J. M.; Barthélémy, A.; Fert, A.; Contour, J . P.; Montaigne, F.; Seneor, P. *Science* **1999**, *286*, 507−509.
(20) Velev, J. P.; Belashchenko, K. D.; Stewart, D. A.; van Schilfgaarde, M.; Jaswal, S. S.; Tsymbal, E. Y. *Phys. Rev. Lett.* **2005**, *95*, No. 216601.
(21) Steinle-Neumann, G.; Stixrude, L.; Cohen, R. E. *Proc. Natl. Acad. Sci. U.S.A.* **2004**, *101*, 33−36.
(22) Battocletti, M.; Ebert, H.; Akai, H. *Phys. Rev. B* **1996**, *53*, 9776−9783.